ORIGINAL ARTICLE

On the Solute Concentration and Corrosion Susceptibility of Mg-xMn-4.0Gd Alloy

Dong-dong Gu[1] · Wen-xing Wu[1] · Shi-kun Xie[1] · Jian Peng[2]

Abstract In this paper, the Fe/Si reduction efficiency, Gd/Mn alloying efficiency, and corrosion susceptibility of the Mg-xMn-4.0Gd alloy were investigated. The results reveal that adding Mn gives a more prominent Fe removal effect under the conventional smelting processes. Neither the amount of Gd addition nor excessive Mn addition is sufficient for the continued strengthening of the Fe removal effect. The alloying efficiency of Mn increased and then decreased as a result of adding Mn alone to mixtures of Mn and Gd elements, while the alloying efficiency of Gd elements gradually diminished. An appropriate amount of Mn addition is beneficial for efficiently improving the corrosion resistance of the alloy. The extruded Mg-0.8Mn-4.0Gd alloy has more outstanding corrosion resistance, with a $CR_{Weighet\ Loss}$ of 4.48 ± 0.33 mg/(cm^2·d) and $CR_{Hydrogen\ Evolution}$ of 2.01 ± 0.31 ml/(cm^2·d). The corrosion susceptibility of the extruded Mg-xMn-4.0Gd alloy mainly hinges on the grain size, Gd solid solubility, and texture intensity of basal plane $I_{(0002)}$.

1 Introduction

Magnesium alloys present impressive performance advantages such as low density and outstanding Bio-compatibility, and are receiving increasing attention in many application fields [1, 2]. However, their weak corrosion resistance seriously limits the widespread application of Mg-based products.

The corrosion behavior of Mg alloy is relevant to the impurities (e.g. Fe, Si, etc.) introduced during the smelting process and to their microstructure. Notably, elemental Fe is one of the impurities that is difficult to completely remove and exists almost throughout the entire life cycle of magnesium alloys. Importantly, the large electrode potential difference between the impurity Fe phase and α-Mg results in the rapid formation of micro-galvanic corrosion in the corrosive medium, which deteriorates the properties of the alloy. Therefore, the impurity Fe content should be controlled at an insufficient level, below its theoretical tolerance limit [3, 4]. With regard to the purification of magnesium alloys, microalloying is expected to control the Fe content in the Mg melt [5–7]. Kim [5] reported that Y has the most vital iron removal ability, which can significantly reduce the corrosion rate of the alloy. The element Mn has been used to remove Fe impurity by forming complex intermetallic compounds such as Mg(or Al)-Fe–Mn in magnesium alloy melts [4]. The corrosion susceptibility of Mg alloys is largely determined by the Fe solid solubility, which can be significantly reduced by addition of manganese and reducing refining temperature. Among the alloying elements capable of achieving a iron removal, Gd is an excellent element for improving corrosion resistance [8–11]. However, there is no research on removing Fe impurities from Mg melts by the combined addition of Gd and Mn. It is also necessary to clarify which part of the alloying process of Gd and Mn elements takes over a more critical part in iron removal. In addition, an in-depth study of the corrosion susceptibility of Mg-Gd-Mn alloy is essential, which can provide significant

✉ Dong-dong Gu
 ddgu1992@sina.com

1 College of Mechanical and Electrical Engineering, Jinggangshan University, Jian 343009, Jiangxi, China

2 College of Materials Science and Engineering, Chongqing University, Chongqing 400044, China

guidance for the design of other Mg alloys with high corrosion resistance requirements.

In this paper, the Fe/Si reduction efficiency and Gd/Mn alloying efficiency of the alloy melts were examined. The microstructure, electrical conductivity, and corrosion rate of the extruded Mg-xMn-4.0Gd alloy were characterized. Detailed analysis was conducted on the influencing factors of corrosion susceptibility of the extruded Mg-xMn-4.0Gd alloy.

2 Experimental

The pure magnesium (0.0050 wt.% Fe, 0.0074 wt.% Si), Mg-Mn intermediate alloy (3.66 wt.% Mn, 0.0123 wt.% Fe, 0.0193 wt.% Si) and Mg-Gd intermediate alloy (24.20 wt.% Gd, 0.0254 wt.% Fe, 0.0302 wt.% Si) were melted in a low-carbon steel crucible under the protection of a protective gas composed of 1 vol.% SF_6 and 99 vol.% CO_2. Insulate the alloy melt at 720 ℃ for 30 min, then scoop out some melt from the half height of the crucible as a sample, and quench in cold water to obtain a solidified ingot. To better illustrate the impurity removal efficiency and alloying efficiency of Mn/Gd elements, Mg-0.8Mn alloy is specially added for comparison. The actual chemical compositions of the alloys were tested by ICP-AES (inductively coupled plasma-atomic emission spectroscopy), as shown in Table 1.

After homogenization annealing, the alloys were extruded into sheets with a size of 5 mm × 60 mm, with an extrusion ratio and extrusion temperature of 19 and 430 ℃, respectively. The microstructure of the alloy was characterized using OM (OPTEC, MDS) and SEM (JEOL JSM-7800F) equipped with EDS. The eddy current conductivity meter (Sigmascope SMP10) was used to detect the conductivity of alloy samples. Corrosion rates were evaluated by measuring the weight loss of alloy samples in a 3.5wt.% NaCl solution at 25 ℃ for 3 days. Meanwhile, H_2 was collected by the acid burette placed upside down above the alloy sample, and the volume of H_2 was calculated by reading the liquid level scale. When the set corrosion time was reached, the corrosion samples were washed in a fume hood with a chromic acid solution at 25 ℃ for about 15 min to remove the corrosion products, and then rinsed quickly with distilled water and dried in cold air. The corrosion rate ($CR_{Weighet Loss}$) and

hydrogen evolution rate ($CR_{Hydrogen Evolution}$) were evaluated using the following formula:

$$CR_{Weight Loss} = \frac{\Delta m}{At} \qquad (1)$$

$$CR_{Hydrogen Evolution} = \frac{\Delta V}{At} \qquad (2)$$

Among them, t is the exposure time (days), and A is the total surface area (cm^2). Δm and ΔV are the metal weight loss (mg) and the measured volume change (ml).

3 Results and Discussion

3.1 Changes in Fe/Si/Gd/Mn Concentration

The purification effect and solute alloying effect of the alloy melt are measured by the actual concentration of Fe/Si/Mn/Gd elements in the design composition. In this chapter, the Fe/Si reduction efficiency is defined as the ratio of the concentration change of Fe/Si to the initial concentration of Fe/Si (theoretical calculation value). The factors that affect Fe/Si reduction efficiency mainly include Fe/Si impurity content, sedimentation process, and the binding of impurity atoms with other atoms. Figure 1a reveals the Fe change and Fe reduction efficiency of the alloy melt at a shorter refining time (30 min). The Fe change of the Mg-0.8Mn alloy melt was 0.00325 wt.% and the Fe reduction efficiency was 44.8%, indicating that the Mn element has a good Fe removal effect at a short refining time. The iron removal effect of the Mg-4.0Gd alloy melt was not satisfactory, with a change in Fe and Fe reduction efficiency of only 0.00014 wt.% and 1.6%, respectively. However, when 0.8 wt.% Mn and 4.0 wt.% Gd were added in coordination, the alloy melt also achieved relatively good iron removal, with a Fe change and Fe reduction efficiency of 0.00238 wt.% and 21.5%, respectively. As the addition of Mn was further increased to 1.0 wt.%, the iron removal effect decreased significantly, as shown by the reduction in iron change and iron reduction efficiency to 0.00017 wt.% and 1.4%, respectively. In short, Mn addition significantly affects the iron removal effect of the Mg melt. The addition of Gd and excess Mn addition within a shorter refining time are not conducive to the continued strengthening of the iron removal effect of the Mg melt.

The alloy melt's Si change and Si reduction efficiency are shown in Fig. 1b. Obviously, the concentration variation trends of Fe and Si elements were entirely inconsistent. A negative value indicates that the actual measured value is higher than the theoretical calculated value. The Mg-0.8Mn alloy melt had the Si change of −0.0329 wt.% and

Table 1 Chemical compositions of Mg-xMn-4.0Gd alloys (wt.%)

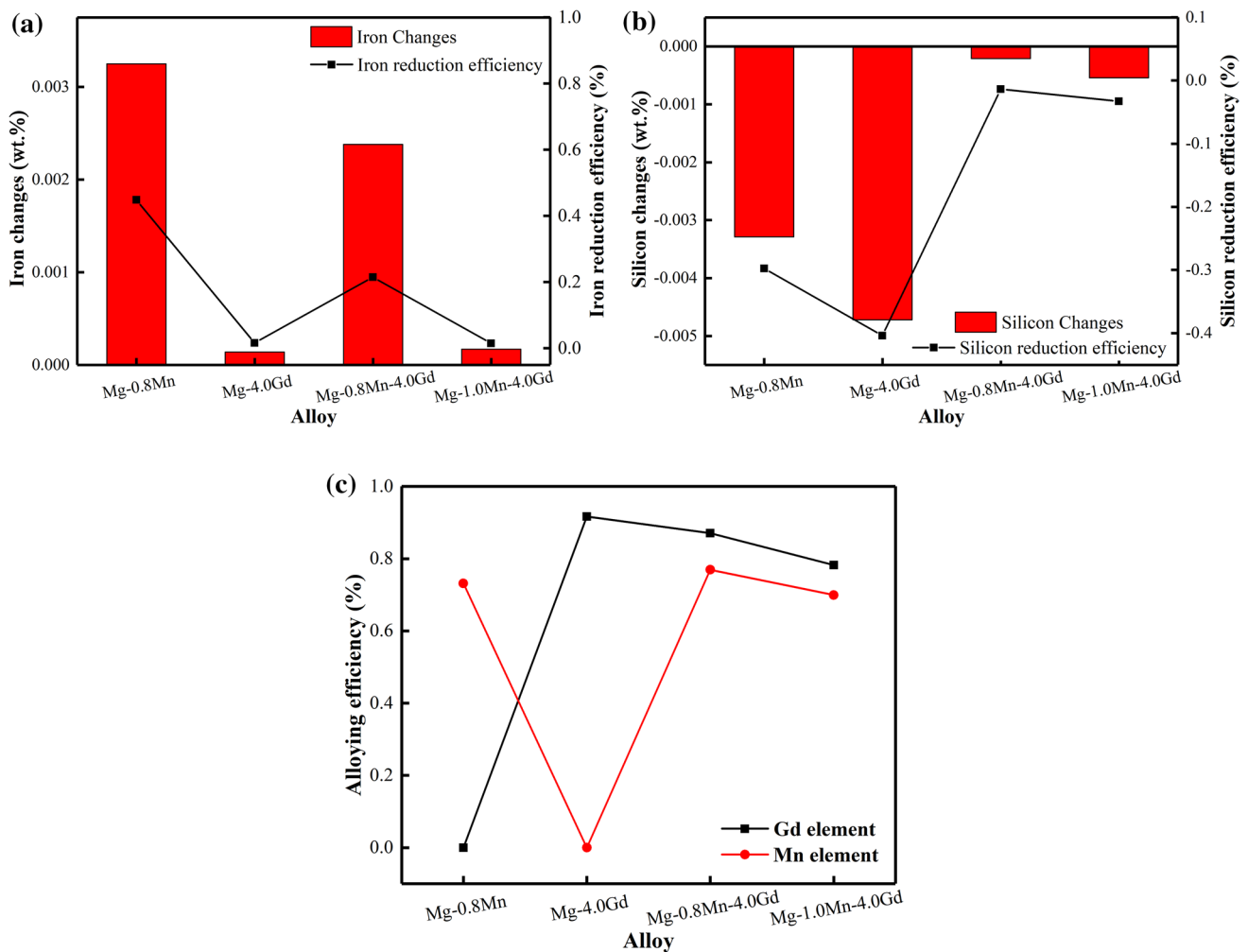| Alloy	Mn	Gd	Fe	Si	Mg
Mg-0.8Mn	0.82	0	0.0047	0.0151	Bal
Mg-4.0Gd	0	4.13	0.0083	0.0169	Bal
Mg-0.8Mn-4.0Gd	0.88	3.99	0.0091	0.0178	Bal
Mg-1.0Mn-4.0Gd	0.98	3.68	0.0142	0.0182	Bal

Fig. 1 **a** The Fe changes /Fe reduction efficiency, **b** Si changes/Si reduction efficiency and **c** alloying efficiency of Gd and Mn elements of the alloy melts

Si reduction efficiency of −29.7%, mainly attributing to the small relative atomic mass of the Si atom and the short settling time. The Mg-4.0Gd alloy melt also showed significant Si change of −0.0472 wt.% and Si reduction efficiency of −40.4%, indicating that it is difficult for the Gd element to achieve prominent Si impurity sedimentation effect within a short refining time. Once Mn and Gd elements were added together, the values of Si change and Si reduction efficiency gradually decreased, meaning that the sedimentation effect of Si impurities slowly came to the fore. However, with the Mn content increasing from 0.8 to 1.0 wt.%, the removal efficiency of impurity Si increased to −3.3%, suggesting that under traditional refining processes, more Mn addition is not conducive to the sedimentation of impurity Si.

During the melting of the alloy, impurities Fe and Si consume part of the alloying atoms, reducing the amount of additions that are truly micro-alloyed. Figure 1c shows the alloying efficiency of the Gd and Mn elements of the alloy

melt. From the addition of Mn alone to the combination of Mn and Gd elements, the alloying efficiency of Mn first increased and then decreased, which was related to the impurity removal of Gd elements and the continuous increase in impurity content. However, the alloying efficiency of the Gd element had continuously decreased, predominantly due to the increase of impurity content. For Mg-0.8Mn-4.0Gd alloy, the alloy melt maintained high alloying efficiencies of Mn (77.0%) and Gd (87.0%).

The iron removal effect of the Mn element is much higher than that of the Gd element, mainly due to the high Gd solid solubility and low Fe solubility [3]. In terms of of the alloying efficiency of the Gd and Mn elements, the addition of Mn alone is more effective on removing iron, and when coupled with Gd, the iron removal efficiency of the melt is significantly lower. This may be due to the solid solubility of Gd/Mn elements in the Mg matrix and the physical binding of Gd and Mn atoms inhibiting the sedimentation

process of Fe impurity. With the addition of Mn, the alloying efficiency of Gd elements gradually decreased, mainly due to an increase in the amount of intermediate alloy with high Fe impurity content during the alloy melting process. In addition, the melting refining time used in this study was too short, only 30 min. Therefore, it was necessary to extend the alloy refining time in order to make more effective use of the solute Gd/Mn for the removal of impurities and the efficiency of the alloying process.

3.2 Microstructure Characterization

Figure 2 shows the microstructure and EDS results of the bottom of alloy ingot. It can be seen from Fig. 2a and b that there are a large number of black, coarse, high-density, and randomly distributed clusters at the bottom of the alloy ingot. The black clusters of Mg-0.8Mn alloy is considered as Fe-rich particles [7]. Both rod-shaped and granular structures can be observed (seeing in Fig. 2c), and EDS analysis shows that both of them contain Fe element, indicating that they are Fe-containing phases.

The SEM microstructure and EDS line scanning results of the center of the cast Mg-xMn-4.0Gd alloy are shown in Fig. 3. The dendrite spacing of the alloy did not change significantly with the increase of Mn content, indicating that Mn element had no significant grain refinement effect on the cast Mg-4.0Gd alloy. With the addition of 0.8 wt.% Mn, the second phase of Mg-4.0Gd alloy changed from a sparse distribution to a aggregation distribution, and the size and area fraction of the second phases slightly increased. The spectral intensity of Gd and Mn elements in the alloy reached a peak in the same white area, evidencing that Mn may participate in the formation of alloy phases (above Fig. 3b). With the Mn content further increasing to 1.0 wt.%, the trend of the second phase aggregation distribution weakened, and the area fraction of the alloy phases decreased. According to the EDS line scanning results (in Fig. 3c below), the relative content of Gd and Mn atoms in the second phase decreased in the white area, suggesting a decrease in the concentration of atoms involved in the formation of the second phase, which is consistent with the ICP results.

Figure 4 shows the optical microstructure and the corresponding grains size distribution histograms of the extruded Mg-xMn-4.0Gd alloy. The average grain size (AGS) of the extruded Mg-4.0Gd alloy was ~8.72 μm. When 4.0 wt.% Gd was added in combination with 0.8 wt.% Mn and 1.0
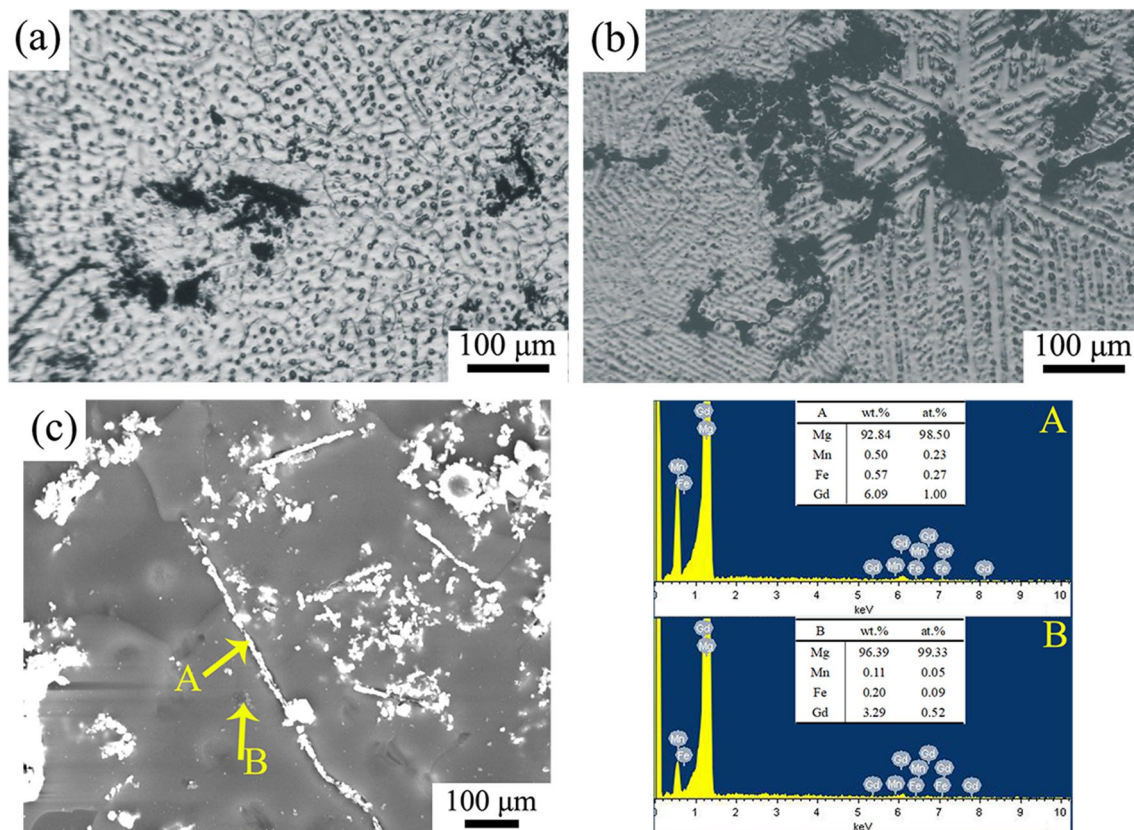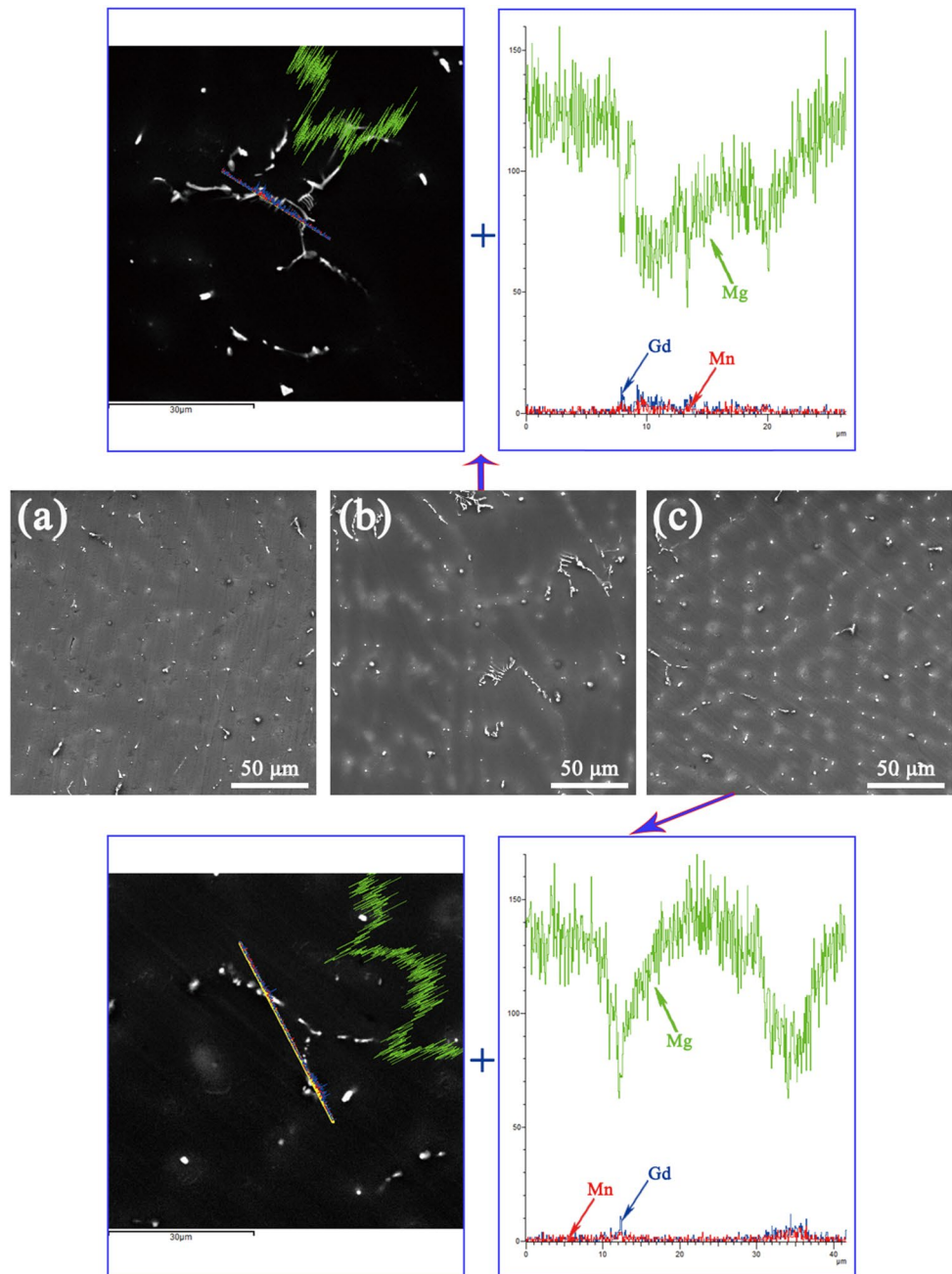

Fig. 2 Optical microstructure, SEM images and EDS results of alloy samples at the bottom of the cast ingot: **a** Mg-0.8Mn; **b** and **c** Mg-0.8Mn-4.0Gd alloy

Fig. 3 SEM images and EDS line scanning results of the center of the as-cast alloy samples: **a** Mg-4.0Gd alloy; **b** Mg-0.8Mn-4.0Gd alloy; **c** Mg-1.0Mn-4.0Gd

wt.% Mn, the grain size distribution range narrowed, and the AGS was decreased to ~ 6.68 and ~ 5.34 μm, respectively. Figure 5 reveals the SEM microstructure and EDS results of the extruded Mg-xMn-4.0Gd alloy. The second phase of the extruded Mg-4.0Gd alloy tended to be randomly distributed, mainly as granular and cubic shapes, with a area fraction of 1.59%. According to literature, the granular phase in the alloys is considered as the Mg_5Gd phase [12, 13]. The Gd content in the cubic-shaped phase is relatively high (seeing in Fig. 5d), which is considered as the Gd rich phase. When 0.8 wt.% Mn was added to the Mg-4.0Gd alloy, the size of the second phase decreased, while the area fraction increased to 1.63%. Based on the EDS results, particle B can be considered the Gd-rich phase. As the Mn content was further increased to 1.0 wt.%, the area fraction of the second phase slightly rose to 1.64%, and the second phase was mainly concentrated at the grain boundaries, which is beneficial for suppressing grain growth. The element Mn could be detected in large particle phases at the grain boundaries (Fig. 5c), which demonstrates that Mn atoms may form a second phase with Mg or Gd atoms.

Figure 6a shows the XRD diffraction patterns of the extruded Mg-xMn-4.0Gd alloy (ED-TD plane). It can be concluded that the composite addition of Mn and Gd did
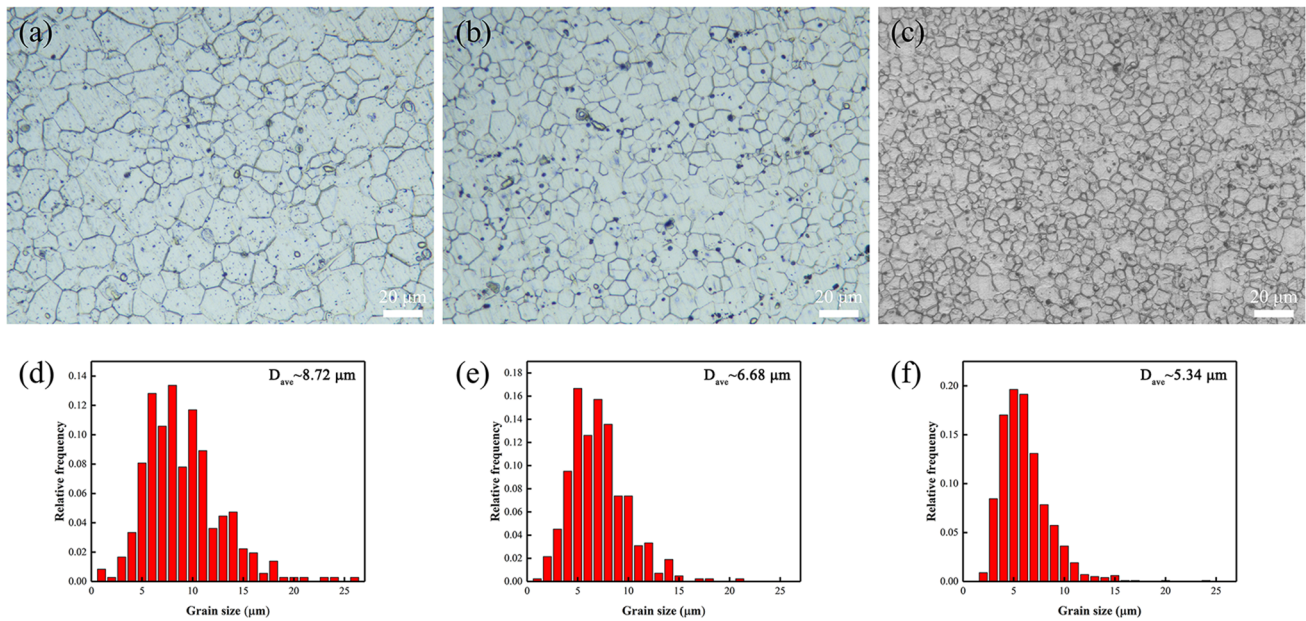
Fig. 4 Optical microstructure and corresponding grains size distribution histogram of the extruded alloy: **a** and **d** Mg-4.0Gd alloy; **b** and **e** Mg-0.8Mn-4.0Gd alloy; **c** and **f** Mg-1.0Mn-4.0Gd alloy
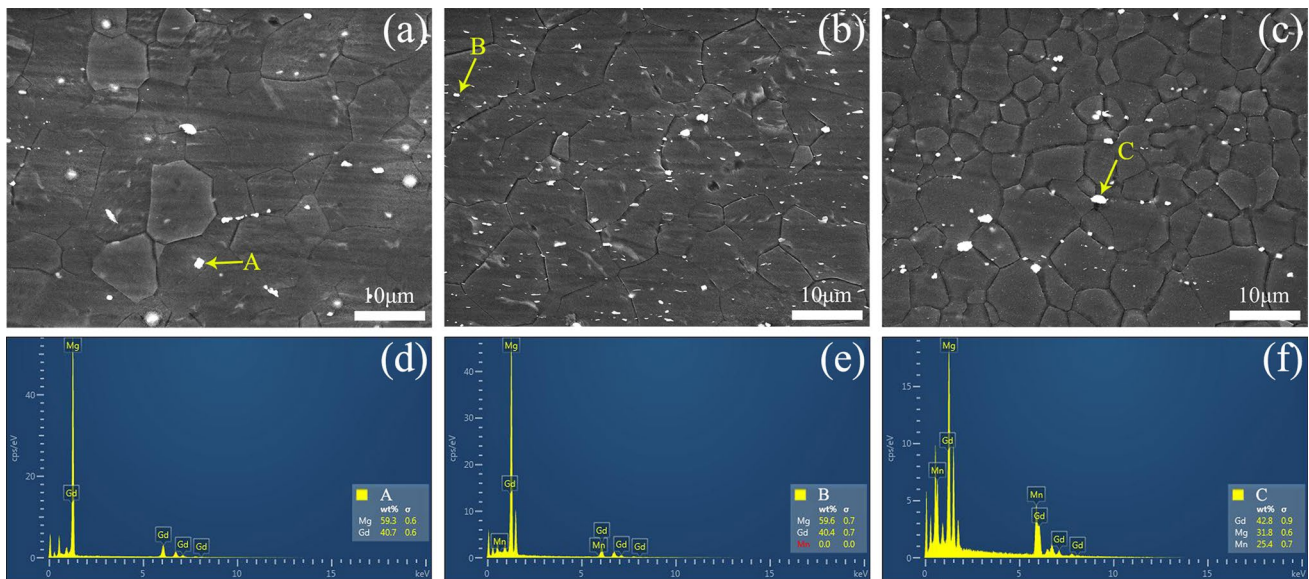

Fig. 5 SEM microstructure and EDS result of the extruded alloys: **a** and **d** Mg-4.0Gd; **b** and **e** Mg-0.8Mn-4.0Gd; **c** and **f** Mg-1.0Mn-4.0Gd

not form any new phases. However, the element Mn can be detected in some MgGd phases, meaning that Mn atoms may dissolve in them. Notably, the presence of impurity phases could not be detected by XRD due to the relatively low content of impurity. Relative intensity ($I_{(hkil)}$) is usually used to evaluate the texture intensity [14]. The three strongest diffraction peaks with 2θ ranging from 30 to 40° represent prismatic plane (10–10), basal plane (0002), and

pyramidal plane (10–11), respectively. The $I_{(0002)}$ was calculated to be 24.3, 18.0 and 25.5% for the extruded Mg-4.0Gd, Mg-0.8Mn-4.0Gd and Mg-1.0Mn-4.0Gd alloys, respectively. This indicates that the Mg-xMn-4.0 Gd alloy did not form a typical extrusion texture, where the basal planes of most grains were parallel to the extrusion direction (ED). With the addition of 0.8 wt.% Mn, the $I_{(0002)}$ of the extruded Mg-4.0Gd alloy decreased, meaning that the basal texture
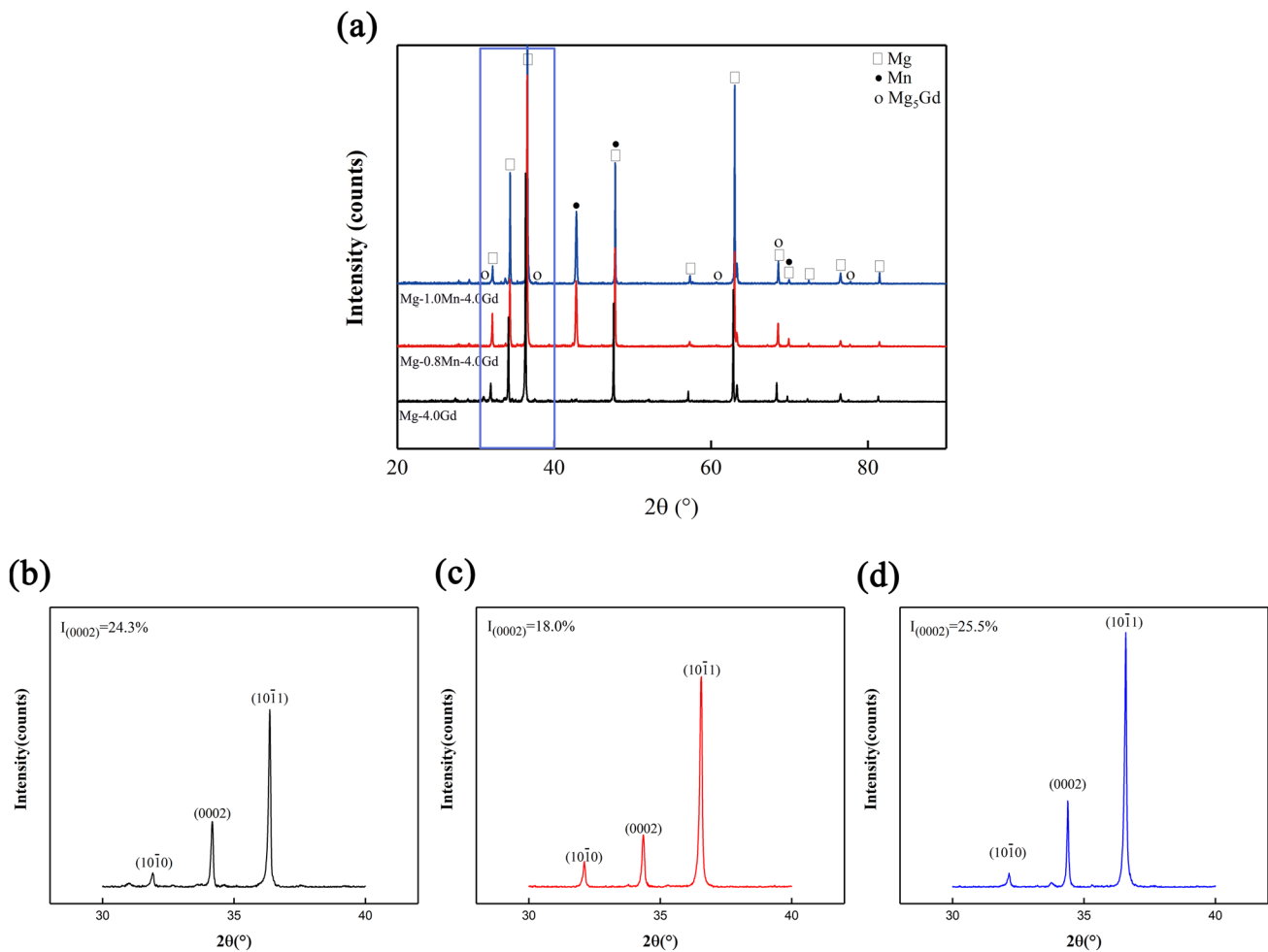
Fig. 6 **a** XRD diffraction patterns of the extruded Mg-xMn-4.0 Gd alloy; **b**, **c** and **d** high magnification of the marked area in (**a**)

was significantly weakened. However, with the Mn content increasing to 1.0 wt.%, the $I_{(0002)}$ increased, indicating that excessive Mn addition might not be conducive to the continuous weakening of the basal texture.

Figure 7a shows the solid solubility of Gd in the Mg matrix. The average solid solubility of the Gd element in the extruded Mg-4.0Gd alloy matrix was 0.47 at.%. With addition of 0.8 wt.% Mn, the average solid solubility of the Gd was increased to 0.53 at.%, mainly due to the fact that during hot extrusion, Mn atoms rapidly precipitated from the Mg matrix and provided more solid solution substitutional position for Gd atoms. However, with the Mn content further increasing to 1.0 wt.%, the average solid solubility of Gd elements dropped to 0.51 at.%, which might be related to the decrease of the actual Gd addition. Figure 7b shows the electrical conductivity of the extruded Mg-xMn-4.0Gd alloy. The solid solubility of components such as Gd, Mn, Fe, and Si in the Mg matrix is a determining factor for the conductivity of the extruded Mg-xMn-4.0Gd alloy. According to the ICP results and alloy phase diagram [15], the main

influencing factor on the electrical conductivity was the Gd solid solubility. The electrical conductivity of the extruded Mg-4.0 Gd alloy was 18.7% IACS, while the electrical conductivity of the alloy decreased to 16.0% IACS with 0.8 wt.% Mn addition, demonstrating an increase in the Gd solid solution of the extruded Mg-0.8Mn-4.0Gd alloy. When the Mn addition continued to increase to 1.0 wt.%, the electrical conductivity of the alloy rose slightly to 16.9%, indicating that the main influencing factor of the alloy's electrical conductivity has shifted to the other factors, such as the second phase. In summary, the electrical conductivity test results are consistent with the alloy solid solubility test results.

3.3 Corrosion Sensitivity Analysis

Figure 8 shows the hydrogen evolution curve and corrosion rate of the extruded Mg-xMn-4.0Gd alloy immersed in 3.5 wt.% NaCl solution for 72 h at 25 ℃. The amount of hydrogen evolution of the alloy continued to rise with increasing immersion time. After adding 0.8 wt.% Mn,
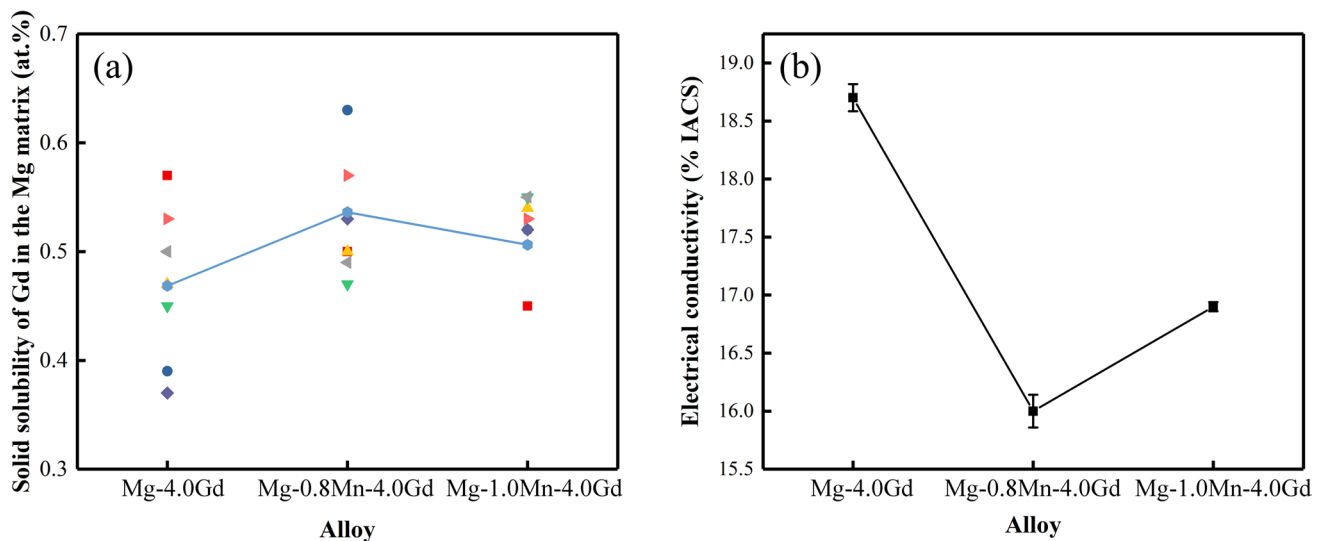
Fig. 7 **a** Solid solubility of Gd element in the Mg matrix and **b** electrical conductivity of the extruded Mg-xMn-4.0Gd alloy
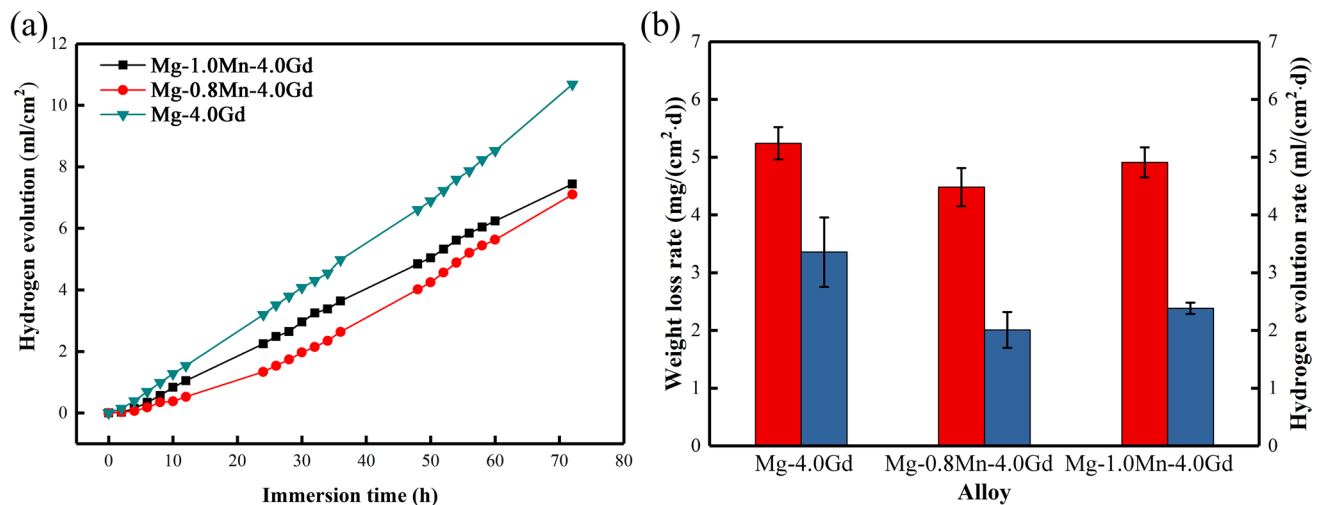

Fig. 8 Hydrogen evolution curve (**a**) and corrosion rate (**b**) of the extruded Mg-xMn-4.0Gd alloy immersed in 3.5 wt.% NaCl solution for 3 days at 25 °C

the hydrogen evolution volume of the alloy significantly decreased. However, as the Mn content further increased to 1.0 wt.%, the hydrogen evolution volume slightly increased, indicating that excessive addition of Mn cannot continuously improve corrosion resistance. The weight loss and hydrogen evolution rates of the extruded Mg-4.0Gd alloy were 5.24 ± 0.28 mg/(cm^2·d) and 3.355 ± 0.6 ml/(cm^2·d), respectively. With the addition of 0.8 wt.% Mn, the weight loss rate and hydrogen evolution rate of the alloy decreased to 4.48 ± 0.33 mg/(cm^2·d) and 2.01 ± 0.31 ml/(cm^2·d), respectively. With the Mn content further increased to 1.0 wt.%, the weight loss and hydrogen evolution rates of the alloy rose to 4.91 ± 0.26 mg/(cm^2·d) and 2.39 ± 0.10 ml/(cm^2·d),

respectively. In summary, reasonable control of Mn addition can effectively improve the corrosion resistance of the alloy.

The corrosion performance of Mg alloys is influenced by the metal contaminants introduced during the melting process (e.g. Fe impurity) and their microstructure. The solute atom Mn of the extruded Mg-xMn-4.0 Gd alloy precipitated almost completely and the area fraction of the second phase hardly changed significantly. Consequently, there are four major factors considered in the corrosion susceptibility analysis of this alloy: iron concentration, average grain size, Gd solid solubility, and $I_{(0002)}$.

The iron impurity concentration of the extruded Mg-xMn-4.0 Gd alloy was lower than 170 ppm, which is a

widely accepted tolerance limit for Fe during the corrosion process [16, 17]. As mentioned, the solid solubility of the impurity element Fe decreases after adding Mn and Gd. The relationship between weight loss rate and iron concentration is indicated in Fig. 9a. The corrosion rate of the alloy first dropped and then rose with the increase of iron concentration, suggesting that the iron concentration was not the main factor affecting the corrosion sensitivity of the extruded Mg-xMn-4.0Gd alloy.

Figure 9b reveals the relationship between weight loss rate and average grain size. Usually, small grain sizes benefit the formation of a continuous film of protective corrosion products, effectively slowing down the corrosion process [18]. The extruded Mg-4.0 Gd alloy had a relatively large grain size of 8.72 μm, which might lead to a higher corrosion rate. As the Mn content increased, the grain size of the alloy

continued to decrease. However, the abnormal increase in the corrosion rate of the extruded Mg-1.0Mn-4.0 Gd alloy might be due to the influence of other factors besides grain size.

As solute Gd atoms dissolved into the magnesium matrix, the potential difference decreased, which is not conducive to the expansion of the corrosion process. The relationship between weight loss rate and solid solubility of Gd is shown in Fig. 9c. As can be seen in the figure, the corrosion rate of the alloy decreased with the increase of Gd solid solubility. This indicates that the solid solubility of Gd solute is also an important factor affecting the corrosion sensitivity of the extruded Mg-xMn-4.0Gd alloy.

In addition, texture is also an important factor affecting the corrosion process of magnesium alloys [19]. Figure 9d presents the relationship between weight loss rate and
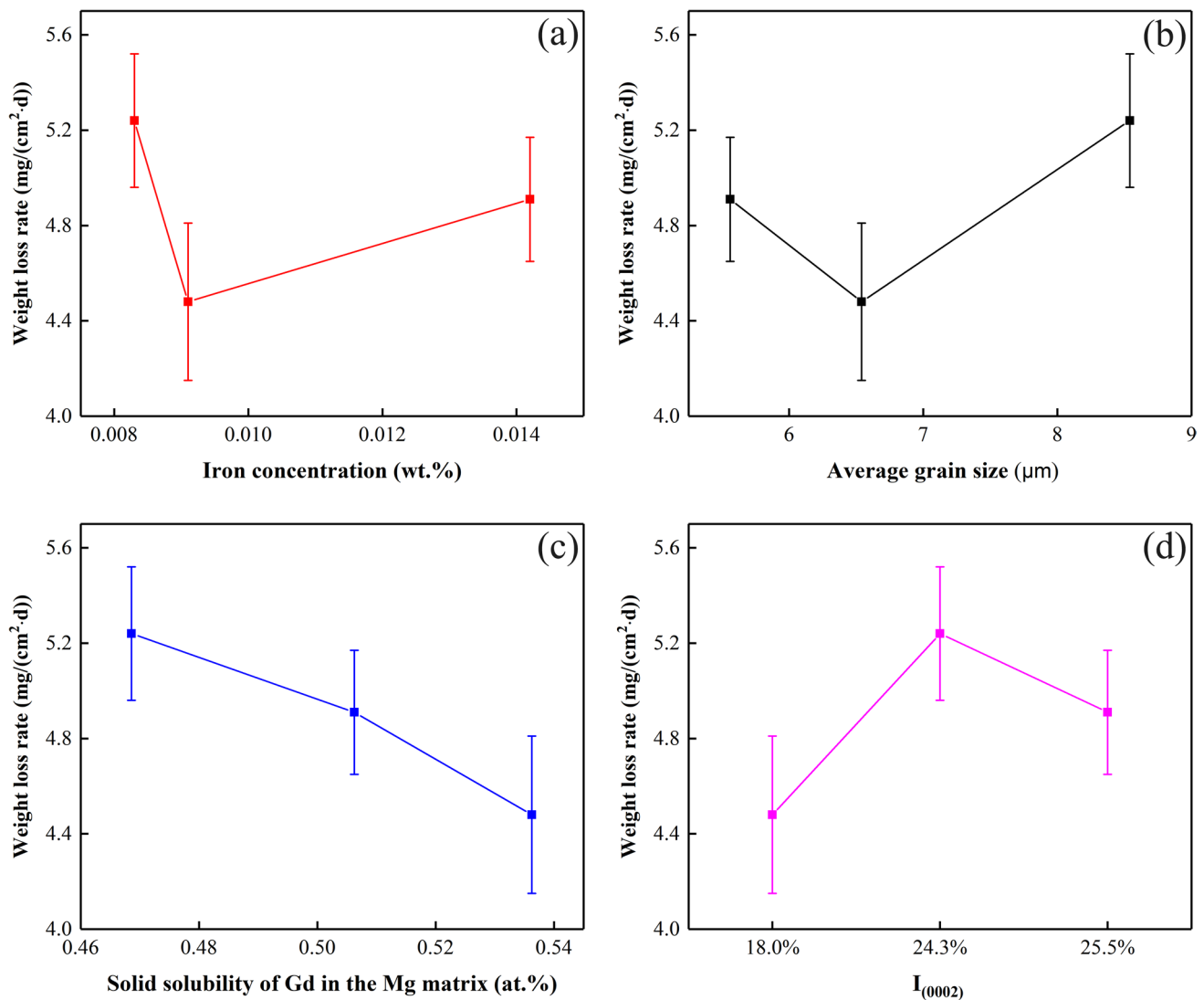

Fig. 9 Relationship between weight loss rate and iron concentration (**a**), average grain size (**b**), solid solubility of Gd in the Mg matrix (**c**), and $I_{(0002)}$ (**d**)

texture intensity of basal plane $I_{(0002)}$. Yang [20] reported that the basal plane corroded significantly slower than the other planes. With the increases in Mn content, the $I_{(0002)}$ of the extruded Mg-4.0Gd alloy first decreased and then increased. The $I_{(0002)}$ of the extruded Mg-0.8Mn-4.0Gd alloy was smaller, leading to a lower corrosion rate. Thus, the corrosion sensitivity of the extruded Mg-xMn-4.0Gd alloy mainly depends on grain size, solid solubility of Gd in the Mg matrix, and $I_{(0002)}$.

4 Conclusions

(1) Mn addition significantly affect on the iron removal effect of the Mg melt. However, the iron removal effect of the melt weakens with the addition of Gd and excessive Mn within a shorter refining time.

(2) Over addition of Mn addition is not conducive to the sedimentation of impurity Si. With the increase of Mn content, the alloying efficiency of Mn first increases and then decreases, while that of Gd elements continues to decline.

(3) Reasonable control of Mn addition can effectively improve the corrosion resistance of the Mg-xMn-4.0Gd alloy. Grain size, the solid solubility of Gd in the Mg matrix, and texture intensity of basal plane $I_{(0002)}$ are the major factor affecting the corrosion sensitivity of the extruded Mg-xMn-4.0Gd alloy.

Declarations

Conflict of interest The authors declare that they have no conflict of interest.

References

1. Cho D H, Avey T, Nam K H, Dean D, and Luo A A, *Acta Biomater* **150** (2022) 442.
2. Sun L X, Bai J, and Xue F, *J Mater Res Technol* **21** (2022) 3961.
3. Liu M, Uggowitzer P J, Nagasekhar A V, Schmutz P, Easton M, Song G L, and Atrens A, *Corros Sci* **51** (2009) 602.
4. Gu D D, Peng J, Wang J W, Liu Z T, and Pan F S, *Acta Metall Sin (Engl Lett)* **34** (2021) 1.
5. Kim J I, Nguyen H N, You B S, and Kim Y M, *Scr Mater* **162** (2019) 355.
6. Jiang S Y, Yuan Y, Wang J, Chen T, Wu L, Chen X H, Jiang B, Tang A T, and Pan F S, *Calphad* **79** (2022) 102503.
7. Gu D D, Wang J W, Chen Y B, and Peng J, *T Nonferr Metal Soc* **30** (2020) 2941.
8. Sun Y H, Wang R C, Peng C Q, and Wang X F, *T Nonferr Metal Soc* **32** (2022) 2494.
9. Li L H, Bao J X, Qiao M L, Tian J, Yang Y Q, Sha J C, and Zhang Z Q, *Mat Sci Eng A* **872** (2023) 144979.
10. Yuan X C, Liu M N, Wei K W, Li F Z, Li X Y, and Zeng X Y, *Mat Sci Eng A* **850** (2022) 143572.
11. Guan F, Jiang W M, Zhang Z, Wang J L, and Li G Y, *Mater Charact* **200** (2023) 112898.
12. Gu D D, Peng J, Sun S, and Pan F S, *J Mater Res Technol* **20** (2022) 2859.
13. Tong X, You G Q, Wang Y C, Wu H, Liu W L, Li P Q, and Guo W, *Mater Sci Eng A* **731** (2018) 44.
14. Guan K, Meng F Z, Qin P F, Yang Q, Zhang D D, Li B S, Sun W, Lv S H, Huang Y D, Hort N, and Meng J, *J Mater Sci Technol* **35** (2019) 1368.
15. Wang Q, Master Thesis, Chongqing University, Chongqing, China (2016)
16. Atrens A, Johnston S, Shi Z M, and Dargusch M S, *Scr Mater* **154** (2018) 92.
17. Liu M, and Song G L, *Corros Sci* **77** (2013) 143.
18. Aung N N, and Zhou W, *Corros Sci* **52** (2010) 589.
19. Xin R L, Li B, Li L, and Liu Q, *Mater Design* **32** (2011) 4548.
20. Yang L, Zhou X R, Curioni M, Pawar S, Liu H, Fan Z Y, Scamans G, and Thompson G, *J Electrochem Soc* **162** (2015) C362.